IJME

Int. J. of Applied Mechanics and Engineering, 2024, vol.29, No.4, pp.121-142
DOI: 10.59441/ijame/191629

NUMERICAL STUDY OF TURBULENT SEPARATED FLOWS IN AXISYMMETRIC DIFFUSERS BASED ON A TWO-FLUID MODEL

B. Kholboev[1*], Z.M. Malikov[2], M.E. Madaliev[3], M. Shoev[2], S. Masharipov[4]

[1]Information System and Mathematical Sciences, Plekhanov Russian University of Economics, UZBEKISTAN
[2]Fluid Mechanics, 1Institute of Mechanics and Earthquake Engineering M.T. Urazbaev, Academy of Sciences of the Republic of Uzbekistan, UZBEKISTAN
[3]Fluid Mechanics, Institute of Mechanics and Earthquake Engineering M.T. Urazbaev, Academy of Sciences of the Republic of Uzbekistan., UZBEKISTAN
[4]Applied Sciences, Tashkent University of Information Technologies, named after Muhammad al-Khwarizmi, UZBEKISTAN
E-mail:bakhodir.kholboev@gmail.com

In this study, numerical simulation of turbulent flow in an axisymmetric diffuser was carried out at Reynolds number Re = 1.56×10^4 and different diffuser expansion angles: $\alpha = 14°$, $18°$ and $90°$. The results obtained were compared with data from previously conducted experiments from the ERCOFTAC database. The inlet flow in the diffuser was considered to be fully developed and turbulent, identical to the experimental data. To simulate the flow, a recently developed two-fluid turbulence model was used in the Comsol Multiphysics 6.2 software package. The study also presented the results of numerical simulations using well-known turbulence models: the two-parameter SST model and the one-parameter SA model, built into the Comsol Multiphysics software package. It was found that the two-fluid turbulence model in the Comsol Multiphysics software package provides more accurate results compared to the considered models. In addition, a higher degree of convergence and stability of this model was noted than the standard turbulence models that are built into Comsol Multiphysics.

Key words: Navier-Stokes equations, axisymmetric diffuser, separated flow, turbulent flow, two-fluid model.

1. Introduction

The description of flow under axisymmetric expansion represents a typical example of turbulent flow, which is widespread in various engineering scenarios. For example, diffusers with different expansion angles are widely used as a hydraulic element in various technical and technological devices. Sudden expansion is also widely used in combustion chamber design. It can act as a flame stabilizer or serve as an element for dissipating instantaneous emissions. Experimental and theoretical studies show that the flow in diffusers is quite complex. Under certain conditions, phenomena such as flow separation, reverse flow and increased turbulence can be observed. Moreover, the flow separation in the diffuser strongly depends on its geometry and flow parameters. For this reason, it is critical to determine whether boundary layer separation from the surface will occur and to precisely determine the location of this separation in the flow. This phenomenon is important both in theoretical and practical aspects, which is confirmed by many studies. Flow separation occurs when the boundary layer overcomes a positive pressure gradient [1-3]. Finding the break-off point is a difficult task. The work of Chebechi *et al.* [4] calculated the separation point in incompressible turbulent flows, where four prediction methods were used: the Goldschmid, Stratford, Head and Chebechi-Smith method. The results obtained were subsequently confirmed experimentally. Researchers such as Knob *et al.* [5] have studied the

* To whom correspondence should be addressed

dynamics of boundary layer separation using PIV (Particle Image Velocimetry) and time-resolved biorthogonal decomposition. Gustavsson [6], Yang *et al.* [7] also experimentally investigated flow separation using PIV, comparing the results with conventional measuring instruments such as hot wire anemometer and Preston tubes. Works that consider flows passing through a backward-facing step are also devoted to the study of flow separation. These studies play a key role in the development of fundamental fluid mechanics and have a wide range of practical applications. All the difficulties associated with the separation and reattachment of a turbulent flow with a positive pressure gradient are observed in this case [8-12]. Similar phenomena also occur in sudden expansion channels [13-16], which is a common phenomenon in various engineering applications such as combustion chambers, aircraft, pipelines, nuclear reactors, turbomachinery heat exchangers, building fairings, etc. A study of flow separation depending on the diffuser cone angle for axisymmetric expansion was carried out in the work of Chandavari *et al.* [13]. Also, experimental and numerical studies based on longitudinal flow separation vortices were studied by Thornblom *et al.* [17].

Stieglmeier M., Tropea C., Weiser N., Nitsche W. [20-21] conducted an experimental study of flow in an asymmetric diffuser with different diffuser angles $(\alpha = 14°,\ 18°$ and $90°)$, and since then their diffuser has become widely recognized as the standard. Many numerical studies of flow in an asymmetric planar diffuser have been carried out using various turbulence models. Dheeraj Sagar, Akshoy Ranjan Paul, Anuj Jain [22] used the *k*-ε turbulent model. Although interest in the study of flows has led to many experimental and numerical studies of their fields, as well as their influence on heat and mass transfer coefficients, turbulent properties, especially in regions of recirculating flow, have not been studied in sufficient detail.

Relatively recently, a work was published in which a new approach to describing turbulence was proposed [23]. In this work, it was shown that turbulent flow can be described as a heterogeneous mixture of two fluids with different velocities. Thus, a mathematical model of turbulence was built based on the dynamics of two fluids. In this work, it was revealed that the main difference between the two-fluid approach and the Reynolds approach is that the two-fluid approach leads to a closed system of equations, while the Reynolds approach describes an open system of equations. In [24-26], solutions to various turbulence problems were obtained based on the two-fluid model. These studies demonstrated the ability of the model to describe thermodynamics in a free turbulent jet, in a rotating flow, and also in flow around a plate. The study showed that the two-fluid turbulence model has high accuracy, ease of application in engineering problems, and the ability to adequately describe turbulence anisotropy.

Therefore, the purpose of this work is to validate the two-fluid turbulence model and verify the computational algorithm on a number of simple test problems, axisymmetric expansion with different semi-angles of the diffuser $(\alpha = 14°,\ 18°$ and $90°)$ and compare the results obtained with the results of the known turbulence models SST [27] and SA [28, 29] (which are built into the COMSOL Multiphysics program) and experimental data [15, 35].

2. Physical and mathematical formulation of the problem

This study focuses on the systematic analysis of separated flow under axisymmetric expansion with different values of diffuser half-angles, as presented in Fig.1. The geometric parameters of the diffuser are given in Tab.1. The work investigates turbulent flow in a diffuser with half-angle expansion $\alpha = 14°,\ 18°$ and $90°$ at Reynolds number $\mathrm{Re} = 1.56 \times 10^4$. The obtained numerical results are compared with experimental data [15].

Table 1. Geometric parameters of an axisymmetric diffuser.

Step height (*h mm*)	Half angle (α°)	Base length (*x mm*)
15	*14*	*60*
15	*18*	*46.17*
15	*90*	*0.0*

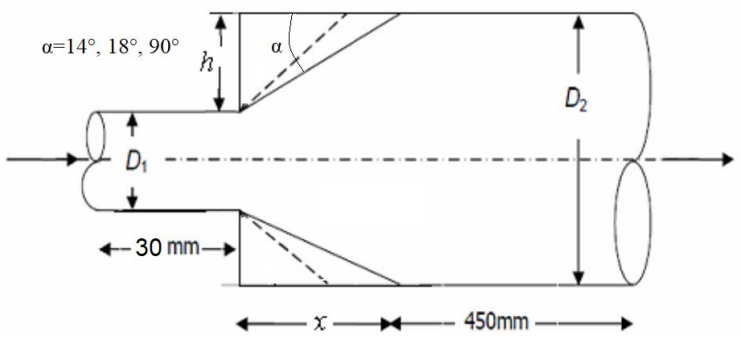

Fig.1. Scheme of the computational domain in an axisymmetric diffuser.

To describe the motion of a turbulent fluid in an axisymmetric diffuser, as mentioned earlier, a two-fluid turbulence model was used. The unsteady system of turbulence equations according to the two-fluid model in a cylindrical coordinate system has the following form [17]:

$$
\begin{cases}
\dfrac{\partial \rho}{\partial \tau}+\dfrac{\partial \rho V_z}{\partial z}+\dfrac{\partial \rho V_y}{\partial r}=0, \\
\rho\dfrac{\partial V_z}{\partial \tau}+\rho V_z\dfrac{\partial V_z}{\partial z}+\rho V_r\dfrac{\partial V_z}{\partial r}+\dfrac{\partial p}{\partial z}= \\
=\nu\rho\left(\dfrac{\partial}{\partial r}\left(\dfrac{\partial V_z}{\partial r}+\dfrac{\partial V_r}{\partial z}\right)+\dfrac{1}{r}\left(\dfrac{\partial V_z}{\partial r}+\dfrac{\partial V_r}{\partial z}\right)+2\dfrac{\partial^2 V_z}{\partial z^2}\right)-\dfrac{\partial \rho\vartheta_z\vartheta_z}{\partial z}-\dfrac{\partial r\rho\vartheta_z\vartheta_r}{r\partial r}, \\
\rho\dfrac{\partial V_r}{\partial \tau}+\rho V_z\dfrac{\partial V_r}{\partial z}+\rho V_r\dfrac{\partial V_r}{\partial r}+\dfrac{\partial p}{\partial r}= \\
\nu\rho\left(2\dfrac{\partial^2 V_r}{\partial r^2}+2\dfrac{\partial V_r}{r\partial r}+\dfrac{\partial}{\partial z}\left(\dfrac{\partial V_z}{\partial r}+\dfrac{\partial V_r}{\partial z}\right)-2\dfrac{V_r}{r^2}\right)-\dfrac{\partial \rho\vartheta_z\vartheta_r}{\partial z}-\dfrac{\partial r\rho\vartheta_r\vartheta_r}{r\partial r}, \\
\rho\dfrac{\partial \vartheta_z}{\partial \tau}+\rho V_z\dfrac{\partial \vartheta_z}{\partial z}+\rho V_r\dfrac{\partial \vartheta_z}{\partial r}=-\left(\vartheta_x\rho\dfrac{\partial V_z}{\partial z}+\vartheta_r\rho\dfrac{\partial V_z}{\partial r}\right)+C_s\rho\left(-\left(\dfrac{\partial V_r}{\partial z}-\dfrac{\partial V_z}{\partial r}\right)\vartheta_r\right)+ \\
+\dfrac{\partial}{\partial z}\left(2\rho\nu'_{zz}\dfrac{\partial \vartheta_z}{\partial z}\right)+\dfrac{\partial}{\partial r}\left(\rho\nu'_{zr}\left(\dfrac{\partial \vartheta_z}{\partial r}+\dfrac{\partial \vartheta_r}{\partial z}\right)\right)+\dfrac{\rho\nu'_{zr}}{r}\left(\dfrac{\partial \vartheta_z}{\partial r}+\dfrac{\partial \vartheta_r}{\partial z}\right)-C_r\rho\vartheta_z, \\
\rho\dfrac{\partial \vartheta_r}{\partial \tau}+\rho V_z\dfrac{\partial \vartheta_r}{\partial z}+\rho V_r\dfrac{\partial \vartheta_r}{\partial r}=-\left(\vartheta_z\rho\dfrac{\partial V_r}{\partial z}+\vartheta_r\rho\dfrac{\partial V_r}{\partial r}\right)+C_s\rho\left(\left(\dfrac{\partial V_r}{\partial z}-\dfrac{\partial V_z}{\partial r}\right)\vartheta_z\right)+ \\
+\dfrac{\partial}{\partial z}\left(\rho\nu'_{zr}\left(\dfrac{\partial \vartheta_r}{\partial z}+\dfrac{\partial \vartheta_z}{\partial r}\right)\right)+\dfrac{\partial}{\partial r}\left(2\rho\nu'_{rr}\dfrac{\partial \vartheta_r}{\partial r}\right)+\dfrac{2\rho\nu'_{rr}}{r}\dfrac{\partial \vartheta_r}{\partial r}-2\rho\nu'_{rr}\dfrac{\vartheta_r}{r^2}-C_r\rho\vartheta_r.
\end{cases}
\tag{2.1}
$$

Here $\nu'_{zz}=\nu'_{rr}=\dfrac{3}{\mathrm{Re}}+2\dfrac{S}{\left|\overline{defU}\right|}$, $\nu'_{zr}=\dfrac{3}{\mathrm{Re}}+2\left|\dfrac{\vartheta_z\vartheta_r}{\overline{defU}}\right|$,

$$\left|\boldsymbol{def}\bar{U}\right| = \sqrt{2\left(\left(\frac{\partial V_z}{\partial z}\right)^2 + \left(\frac{\partial V_r}{\partial r}\right)^2 + \left(\frac{V_r}{r}\right)^2\right) + \left(\frac{\partial V_r}{\partial z} + \frac{\partial V_z}{\partial r}\right)^2},$$

$$S = \frac{\vartheta_z{}^2 J_z + \vartheta_r{}^2 J_r}{J_z + J_r}, \quad J_z = \left|\frac{\partial \vartheta_z}{\partial z}\right|, \quad J_r = \left|\frac{\partial r \vartheta_r}{r \partial r}\right|, \quad C_s = 0.2, \quad C_r = C_1 \lambda_{\max} + C_2 \frac{\left|d \cdot \bar{\vartheta}\right|}{d^2}.$$

In the given equations V_z, V_r – respectively the axial and radial components of the averaged flow velocity vector, p – hydrostatic pressure, ϑ_z, ϑ_r – relative axial and radial components of fluid velocity, ν – molar kinematic viscosity, $\nu'_{zz}, \nu'_{rr}, \nu'_{zr}$ – effective molar viscosities, d – closest distance to a solid wall, $\lambda_{\max}$ – largest root of the characteristic equation.

$$\det(A - \lambda E) = 0, \tag{2.2}$$

where is the matrix

$$A = \begin{vmatrix} -\frac{\partial V_z}{\partial z} & -\frac{\partial V_z}{\partial r} - C_s\left(\frac{\partial V_r}{\partial z} - \frac{\partial V_z}{\partial r}\right) \\ -\frac{\partial V_r}{\partial z} + C_s\left(\frac{\partial V_r}{\partial z} - \frac{\partial V_z}{\partial r}\right) & -\frac{\partial V_r}{\partial r} \end{vmatrix}.$$

The largest root of the equation of the characteristic is equal to:

$$D = \frac{\partial V_z}{\partial r}\frac{\partial V_r}{\partial z} - \frac{\partial V_z}{\partial z}\frac{\partial V_r}{\partial r} + C_s(1 - C_s)\left(\frac{\partial V_r}{\partial z} - \frac{\partial V_z}{\partial r}\right)^2,$$

$$\lambda_{\max} = \sqrt{D}, \quad \text{if} \quad D > 0,$$

$$\lambda_{\max} = 0, \quad \text{if} \quad D < 0.$$

The constant coefficients of Eq.(2.1) are equal $C_1 = 0.7825, C_2 = 0.306$.

To numerically implement system [1], it is necessary to select a suitable computational grid. It is known that the numerical solution depends on the quality of the computational mesh [24]. To obtain satisfactory results, it is necessary to increase the mesh density in areas close to hard surfaces. Many turbulence models such as *k*-ω, SST *k*-ω [21], [25] and Reynolds stress methods require a very fine mesh near the wall, which leads to increased computational resources for applying them to engineering problems. In Fig.2, calculation grids are shown.

For axisymmetric diffusers with corners $\alpha = 14°$ and $18°$ a mesh size of 50×300 was used. In the case of an angle $\alpha = 90°$, a mesh size of 50×50 was chosen for the inlet part of the channel, while a mesh size of 100×200 was used for the expanding part.

The initial and boundary conditions were specified as follows:

For all turbulence models, the input flow velocity was taken from the experimental data presented in Fig.3.

No-slip conditions were set on the boundary walls, and a zero-pressure gradient was used at the outlet.

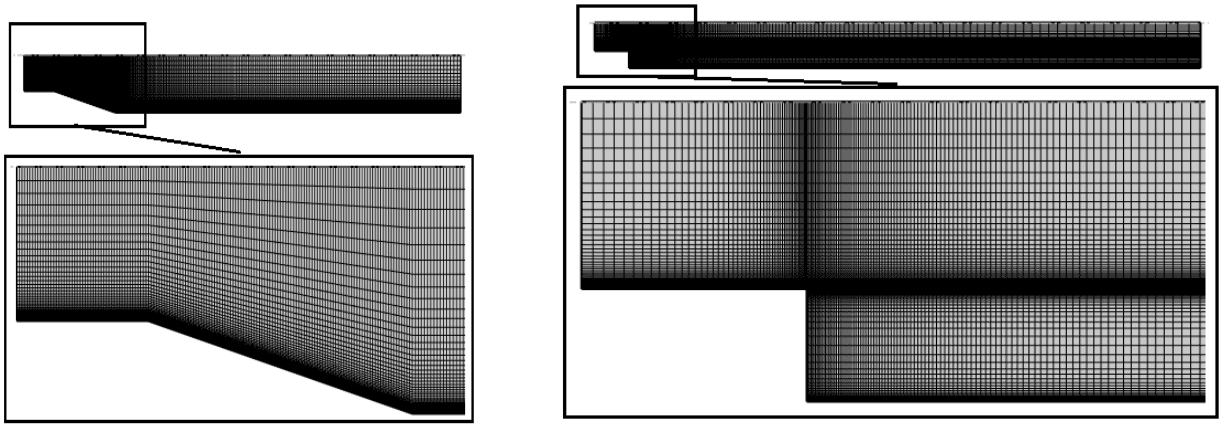

Fig.2. Calculation grids for axisymmetric diffusers.

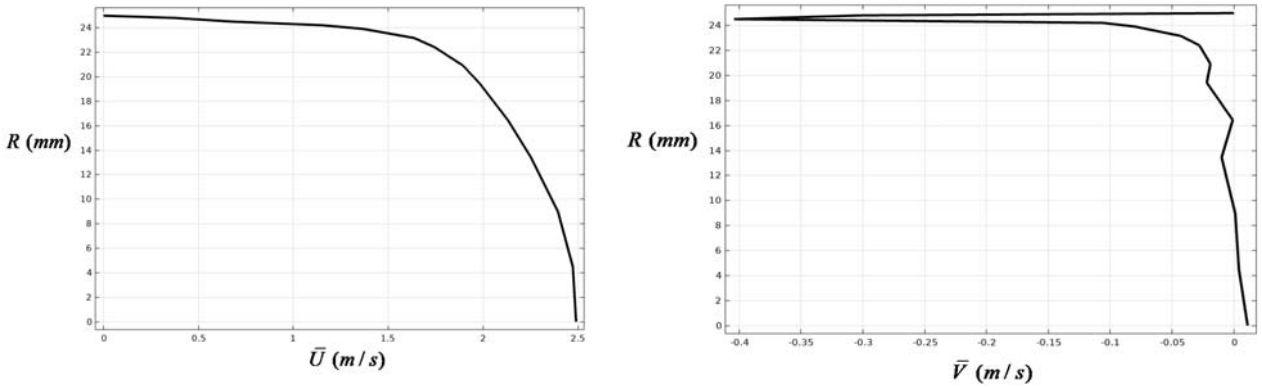

Fig.3. Input flow rate.

3. Solution method

COMSOL Multiphysics provides a variety of solvers to solve a wide range of physics problems. The choice of a particular solver depends on the type of physics being modeled, the complexity of the problem, the required accuracy, and the available computing resources. To solve the two-fluid turbulent model equations, a fully coupled method using the PARDISO direct solver algorithm was chosen in this study. Newton's method with a damping coefficient of *0.1* was chosen as the iteration method. The iterative process continued until *250* iterations were reached. The tolerance factor was set to *1* and the residual factor to *1000*. These parameters play an important role in the solution process and allow us to achieve the necessary balance between calculation accuracy and computational efficiency.

Standard COMSOL Multiphysics solvers were used for the standard SST and SA turbulence models.

4. The discussion of the results

Figures 4-6 show graphs comparing calculated and experimental data for an axisymmetric diffuser with $\alpha = 14°$. For comparison, these plots also show the numerical results obtained using the SST and SA turbulence models. Figure 4 shows the profiles of the axial *U*-component of velocity; Fig.5 profiles of the radial *V*-velocity component and Fig.6 profiles of flow pulsation *u'v'* in various sections.

From Fig.4 you can see that for the initial sections at $x = 0(mm)$ and $x = 10(mm)$ the results of all models are approximately the same. However, starting from $x = 20(mm)$ and in all subsequent sections, the

results of the SST and SA models significantly diverge from the experiment, while the results of the two-fluid model show good agreement with the experimental data.

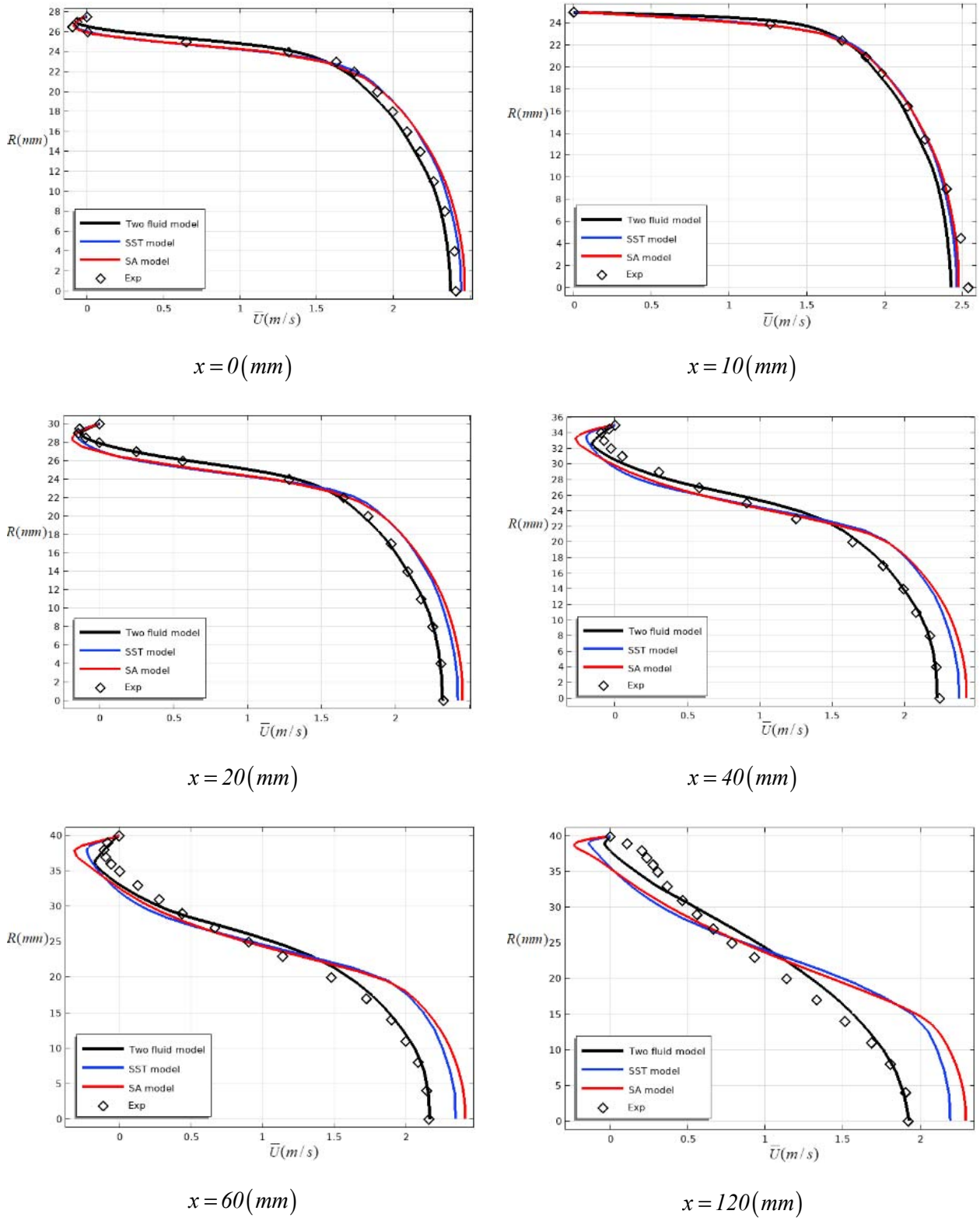

Fig.4. Profiles of the axial *U*-component of the flow velocity.

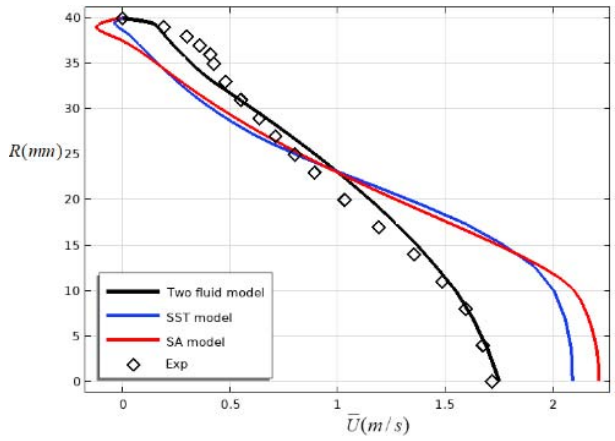

$x = 160(mm)$

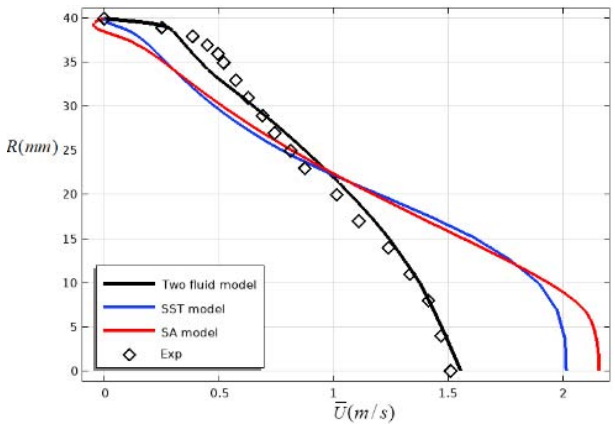

$x = 200(mm)$

Cont. Fig.4. Profiles of the axial *U*-component of the flow velocity.

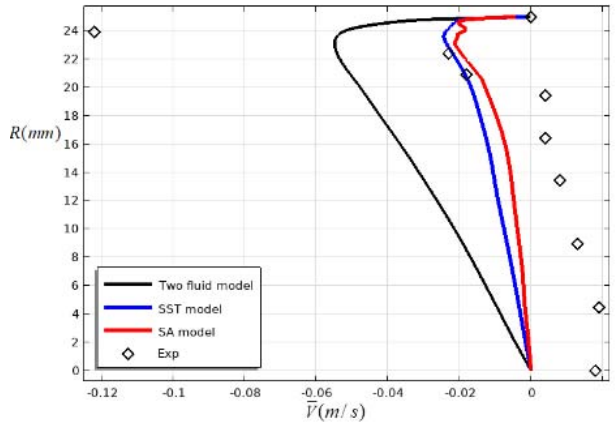

$x = 0(mm)$

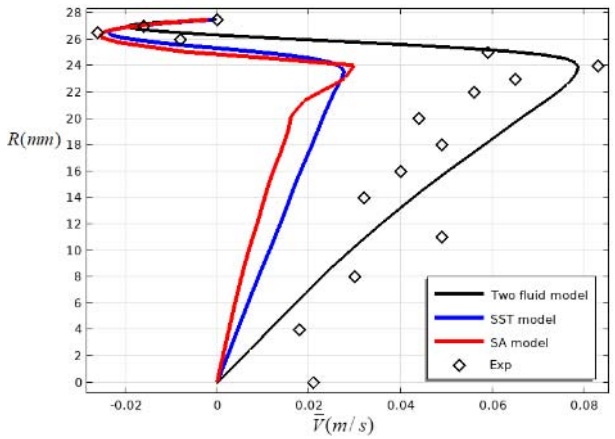

$x = 10(mm)$

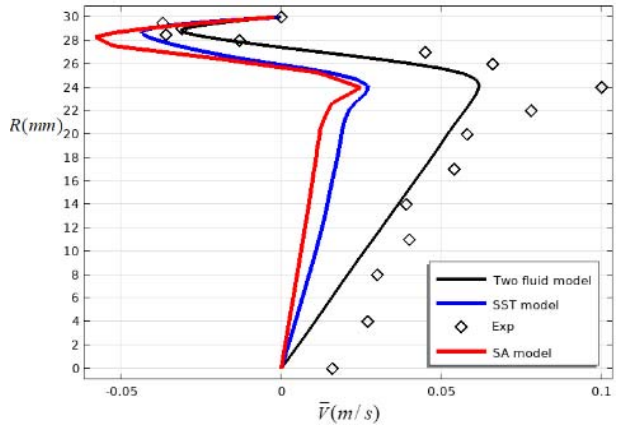

$x = 20(mm)$

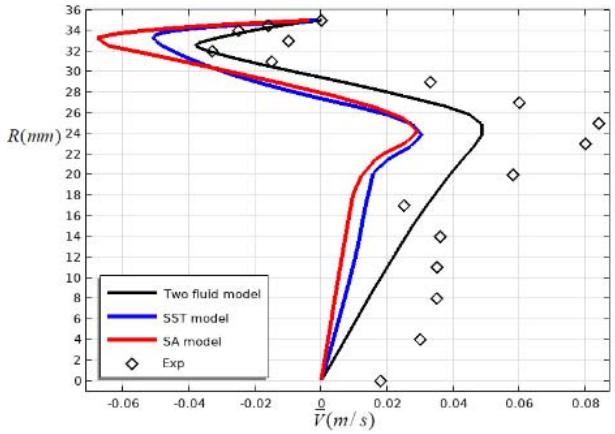

$x = 40(mm)$

Fig.5. Profiles of the radial *V*-component of the flow velocity.

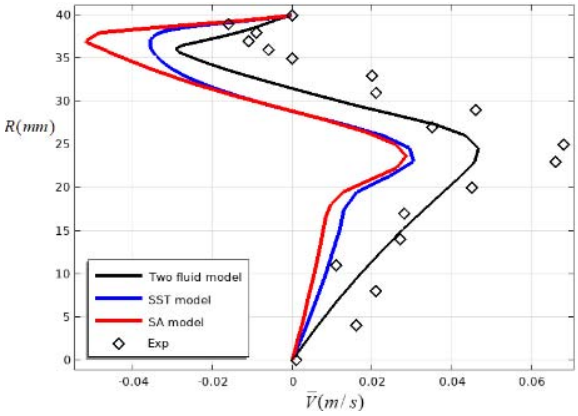

$x = 60(mm)$

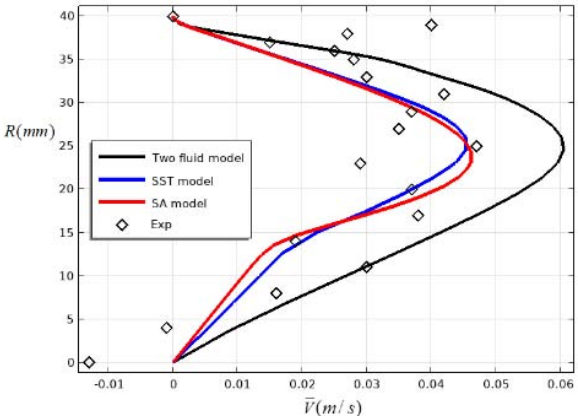

$x = 120(mm)$

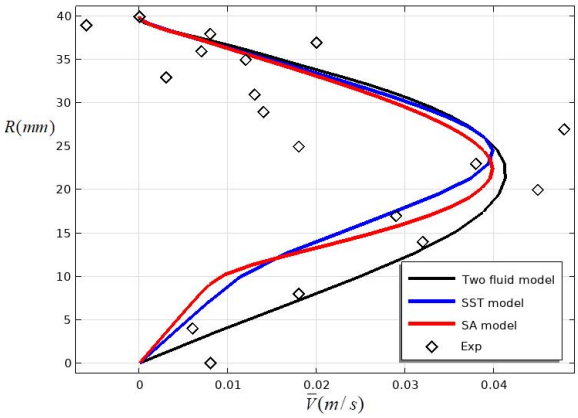

$x = 160(mm)$

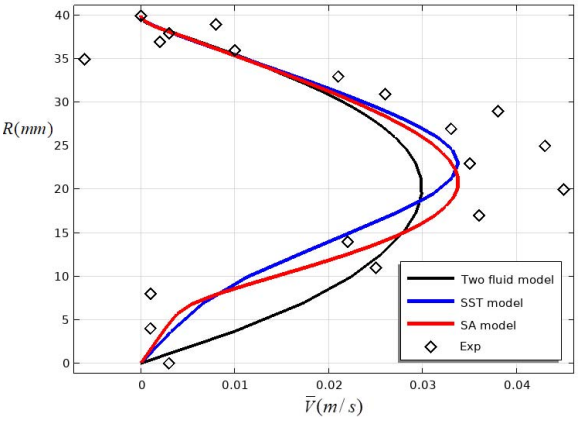

$x = 200(mm)$

Cont. Fig.5. Profiles of the radial *V*-component of the flow velocity.

In a turbulent flow, it is extremely difficult to measure the radial velocity of the flow, which is clearly visible in Fig.5. Therefore, the correspondence of the numerical results with the experimental data is of a qualitative nature.

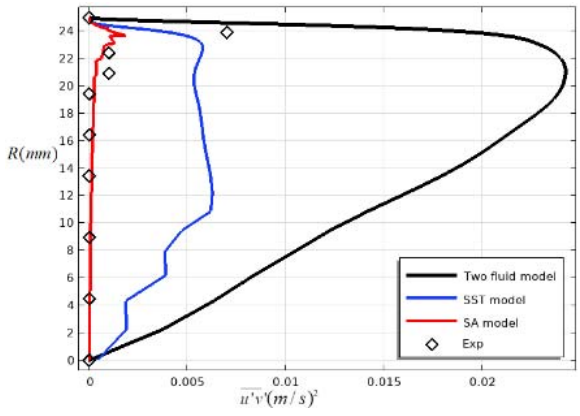

$x = 0(mm)$

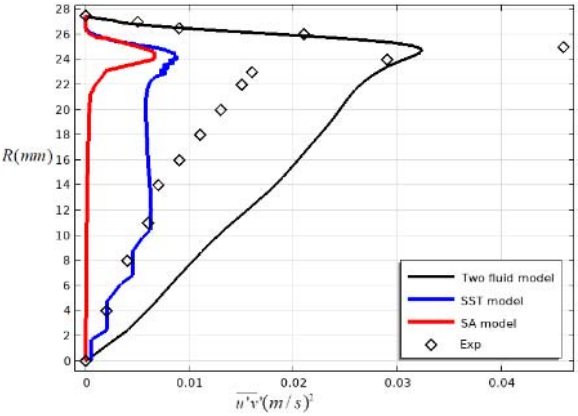

$x = 10(mm)$

Fig.6. Flow pulsation profiles *u'v'*.

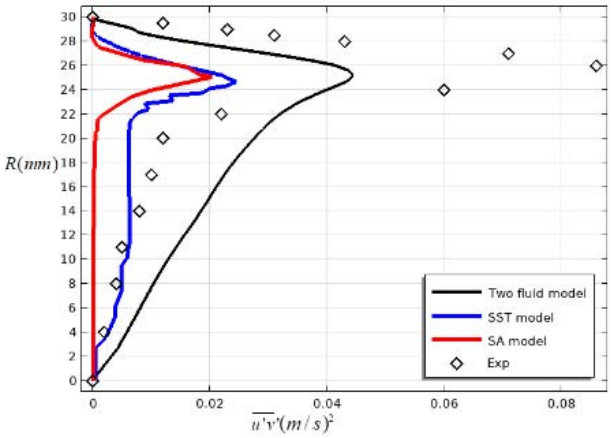

$x = 20(mm)$

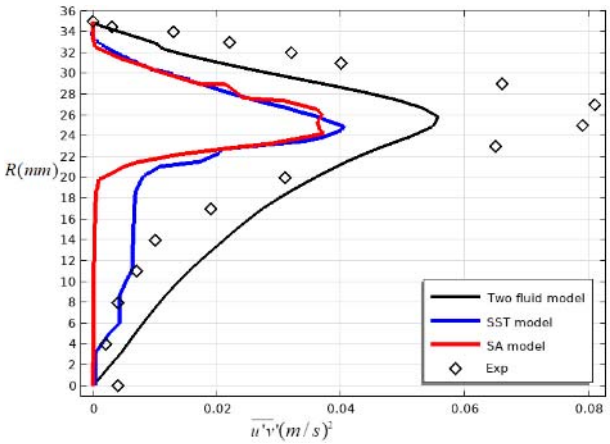

$x = 40(mm)$

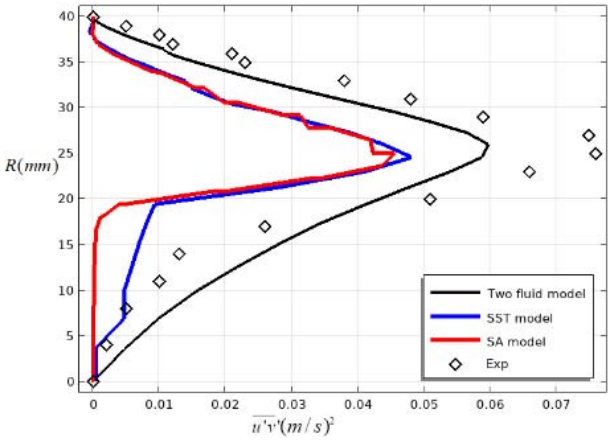

$x = 60(mm)$

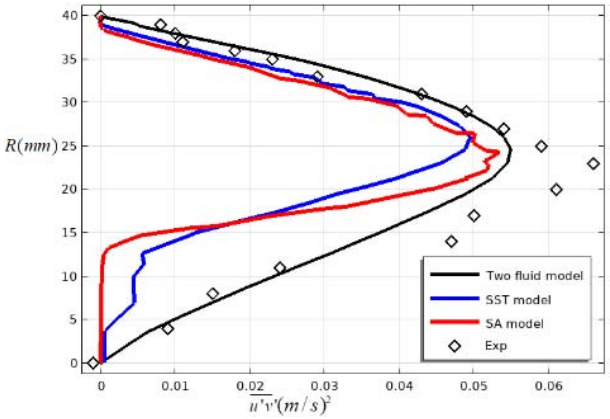

$x = 120(mm)$

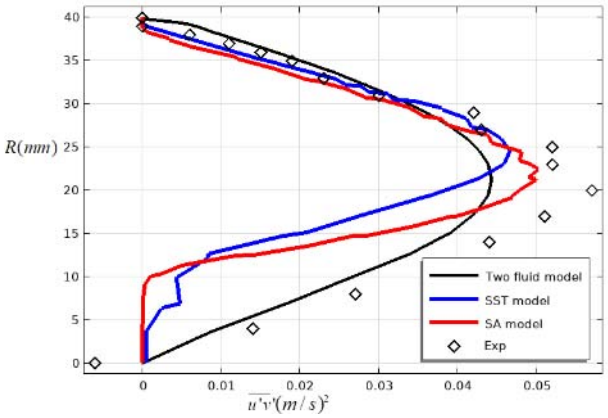

$x = 160(mm)$

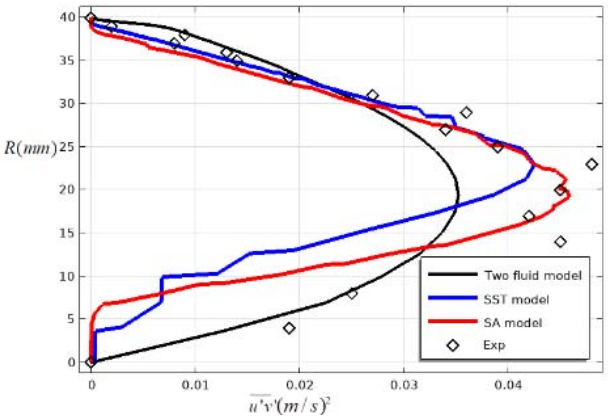

$x = 200(mm)$

Cont. Fig.6. Flow pulsation profiles *u'v'*.

Figure 6 shows profiles for turbulent stresses. From the presented graph it can be seen that the results of the two-fluid model are in fairly accurate agreement with the experimental data, in contrast to the results of the SST and SA models.

Figures 7-9 show comparative graphs of calculated and experimental data for an axisymmetric diffuser with an angle $\alpha = 18°$. For a clearer comparison, numerical results from the SST and SA turbulence models are also presented. Figure 7 shows the profiles of the axial *U*-component of the velocity, Fig.8 shows the profiles of the radial *V*-component of the velocity, and Fig.9 shows the profiles of the flow pulsation *u'v'*-velocity component in various sections.

The numerical results of the models for this diffuser are similar to those for the previous diffuser. Not far from the diffuser entrance, the results of all models are approximately the same. However, as we move away from the entrance, the results of the SST and SA models diverge more and more from the experimental data. As for the two-fluid model, good agreement with experimental data is observed throughout the diffuser.

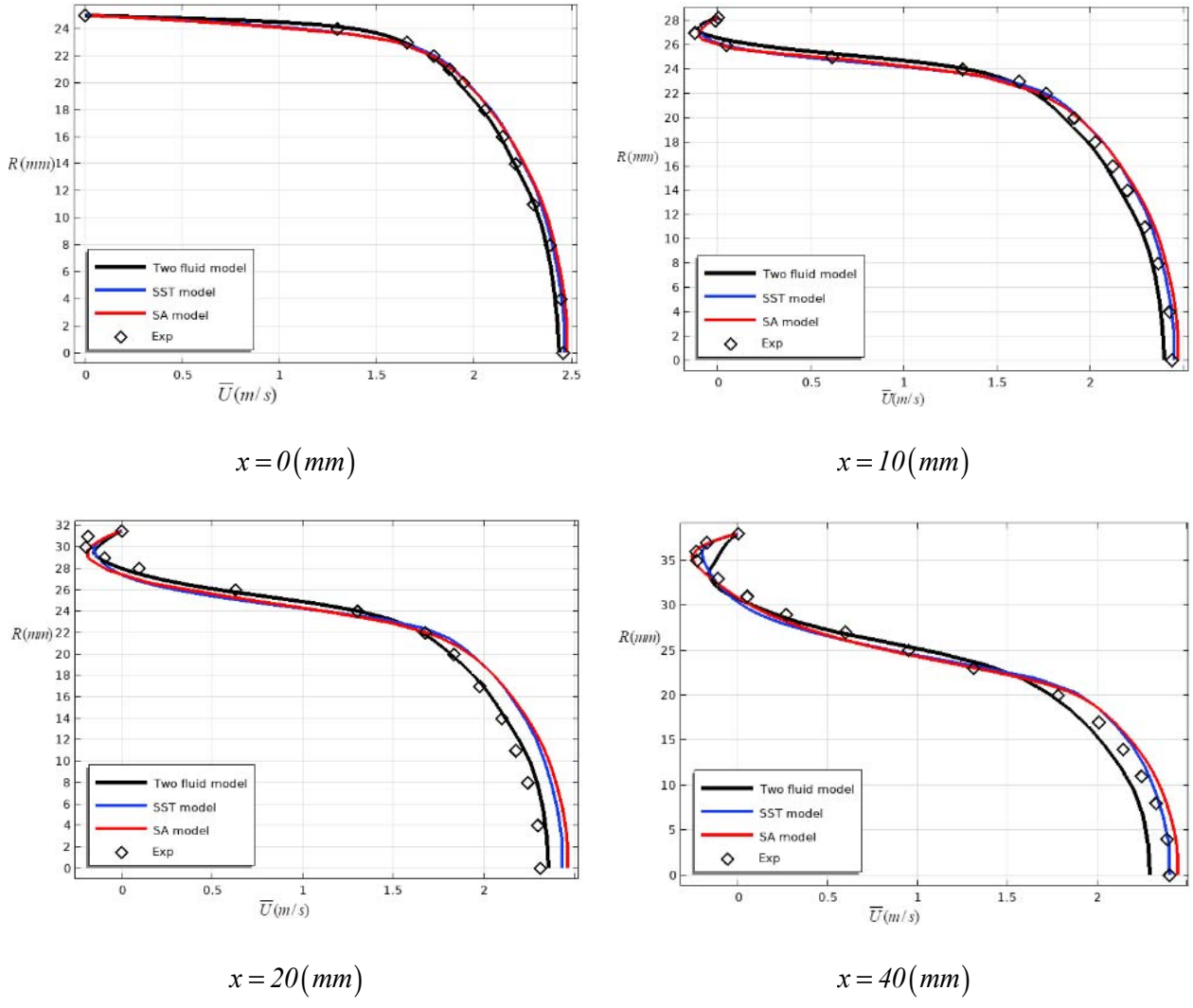

Fig.7. Profiles of the axial *U*-component of flow velocity.

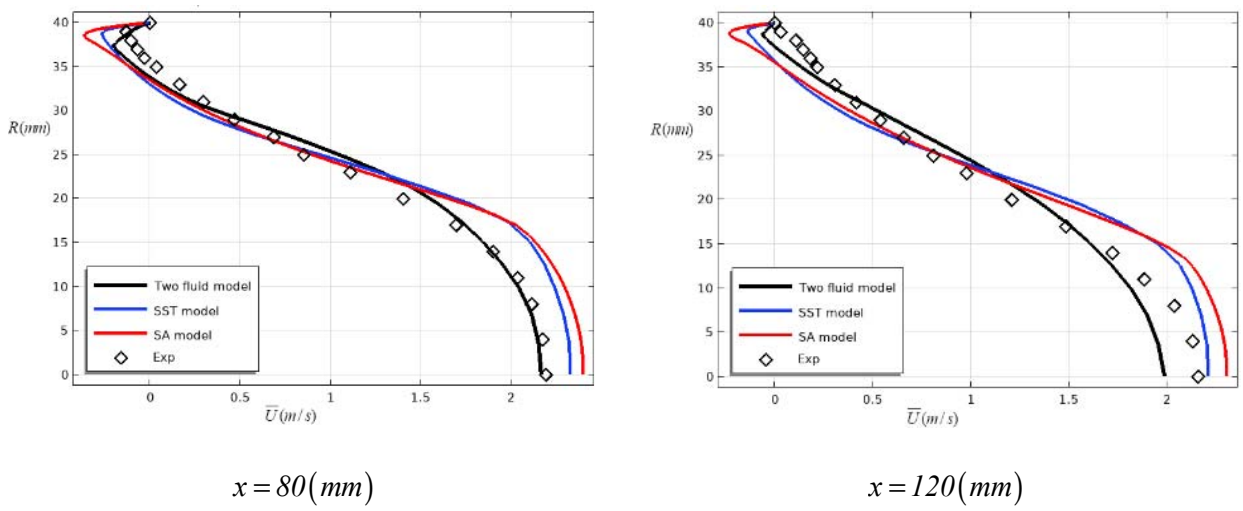

$x = 80(mm)$ $x = 120(mm)$

$x = 160(mm)$ $x = 200(mm)$

Fig.7. Profiles of the axial *U*-component of flow velocity.

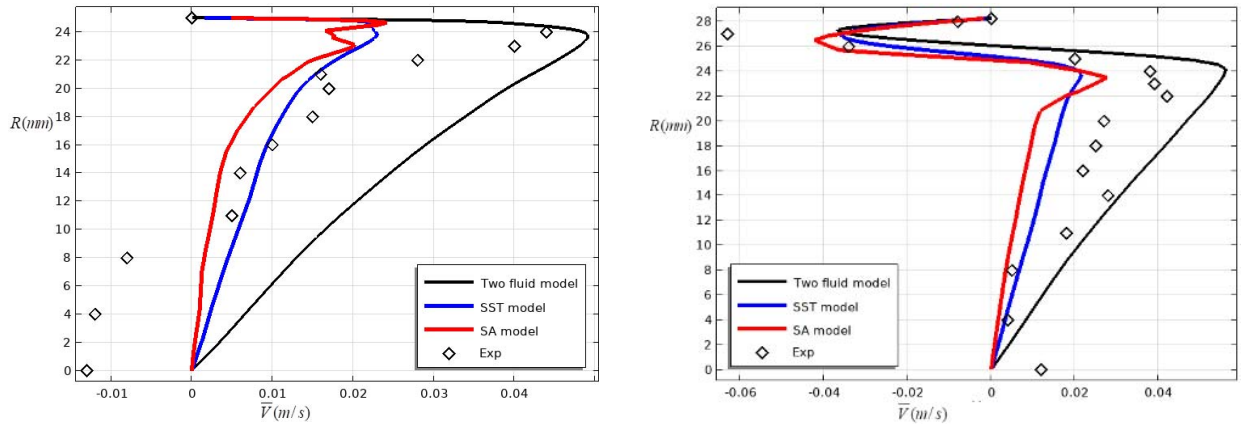

$x = 0(mm)$ $x = 10(mm)$

Fig.8. Profiles of the radial *V*-component of the flow velocity.

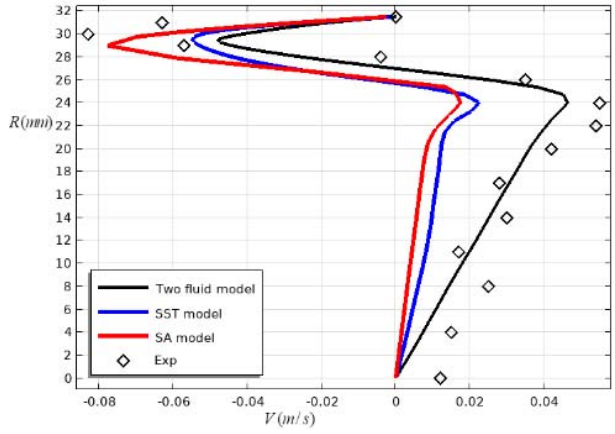

$x = 20(mm)$

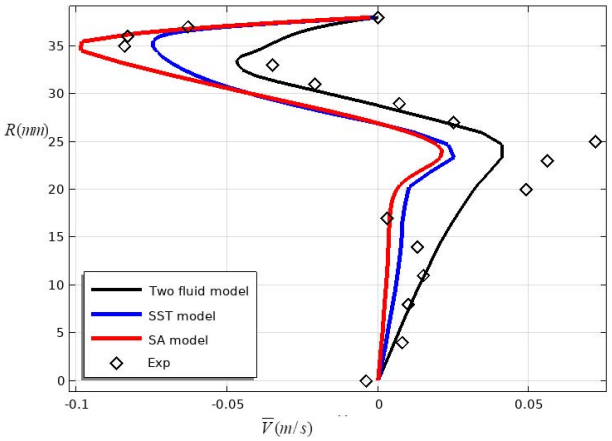

$x = 40(mm)$

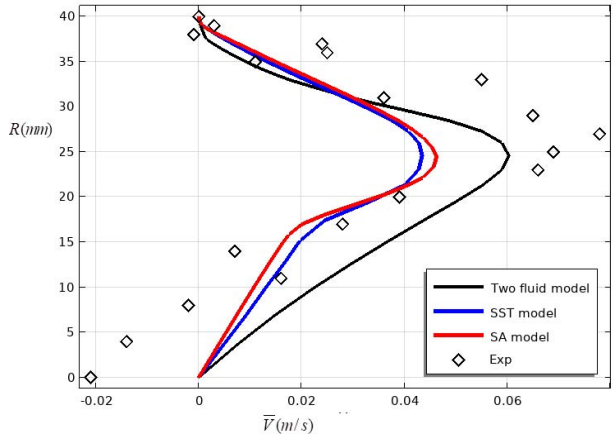

$x = 80(mm)$

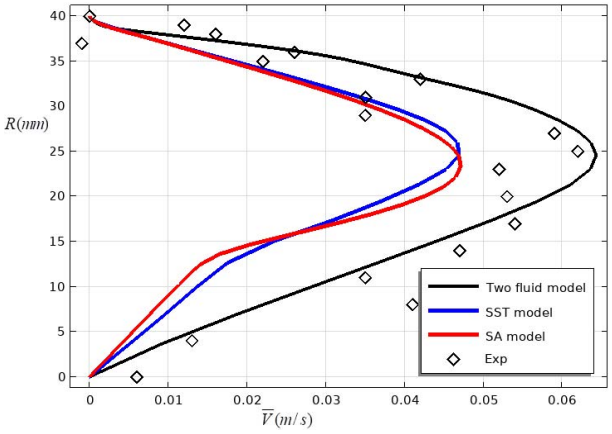

$x = 120(mm)$

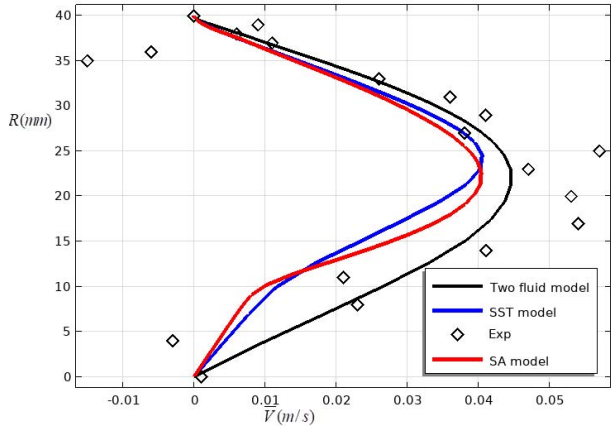

$x = 160(mm)$

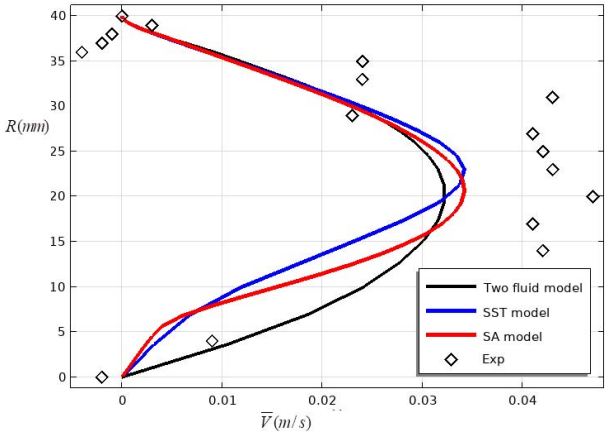

$x = 200(mm)$

Cont. Fig.8. Profiles of the radial V-component of the flow velocity.

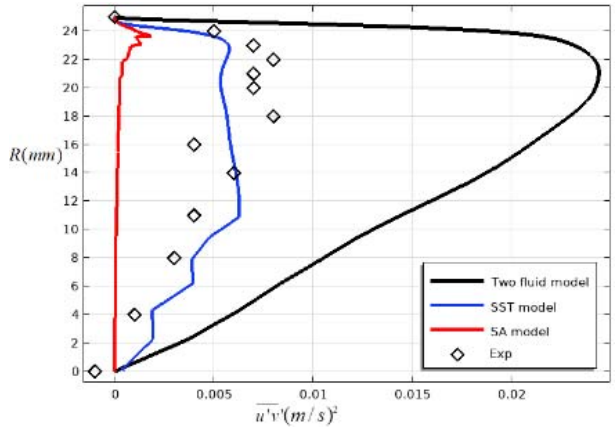

$x = 0(mm)$

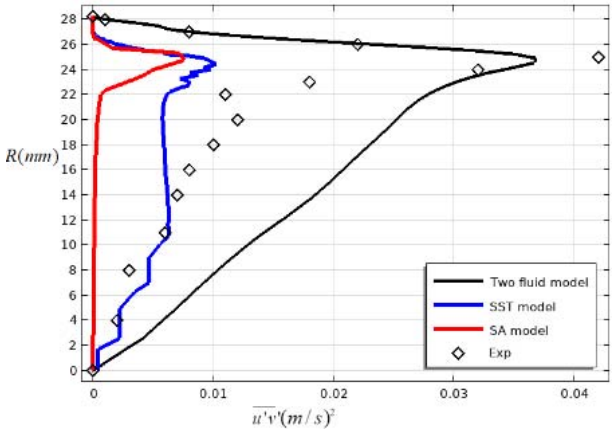

$x = 10(mm)$

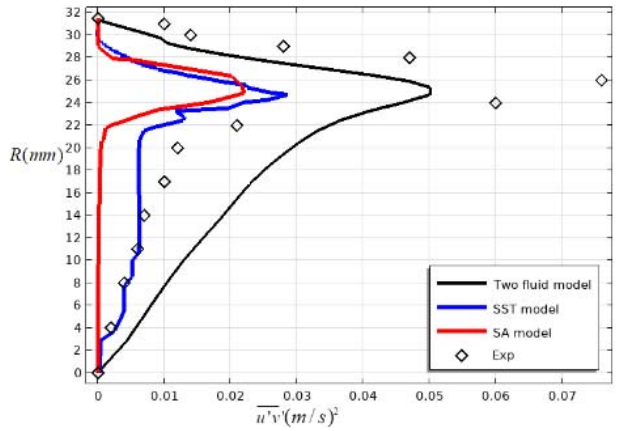

$x = 20(mm)$

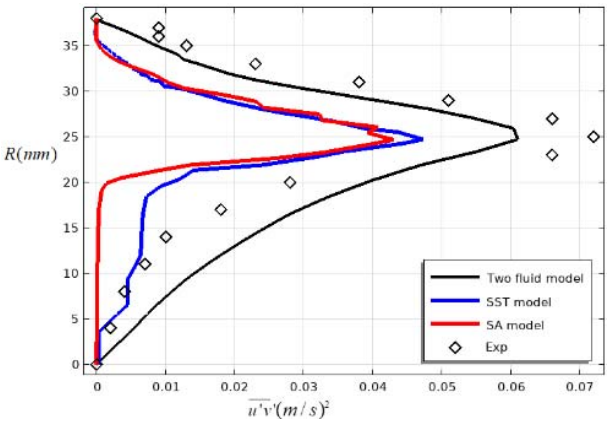

$x = 40(mm)$

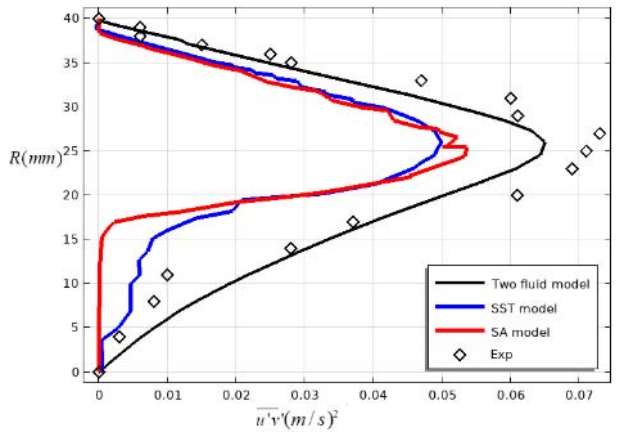

$x = 80(mm)$

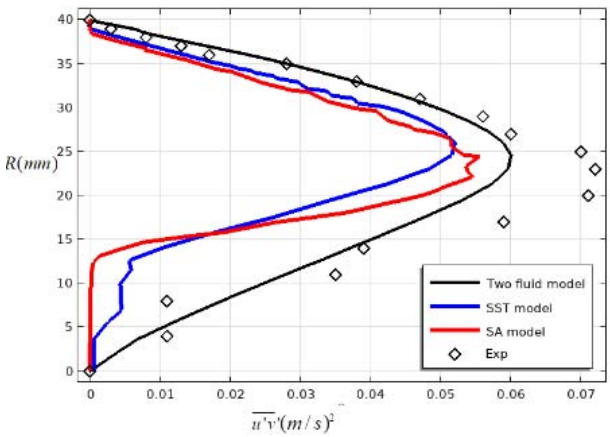

$x = 120(mm)$

Fig.9. Ripple current profiles *u'v'*.

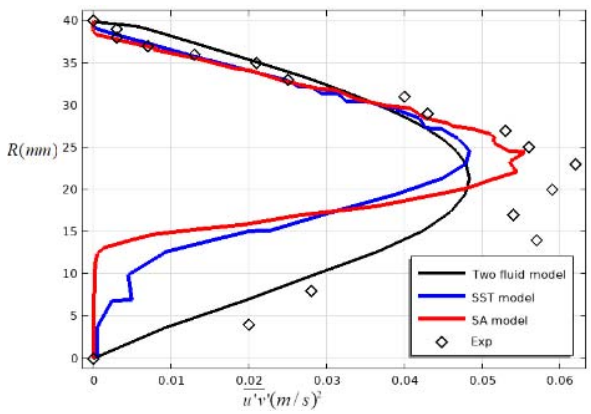

$x = 160(mm)$

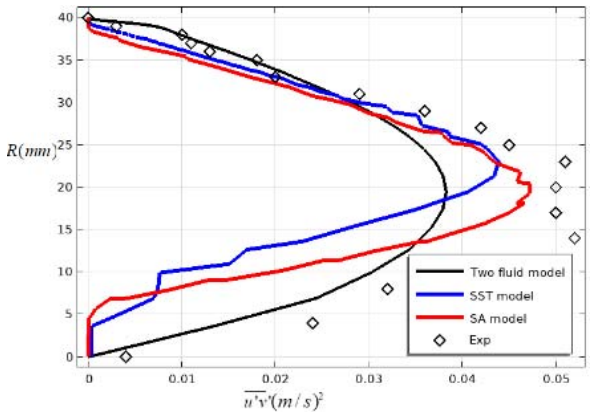

$x = 200(mm)$

Cont. Fig.9. Ripple current profiles *u'v'*.

In Fig.9, showing pulsation profiles, there is also a more adequate agreement between the results of the two-fluid model and experimental measurements, compared to the results of known turbulence models.

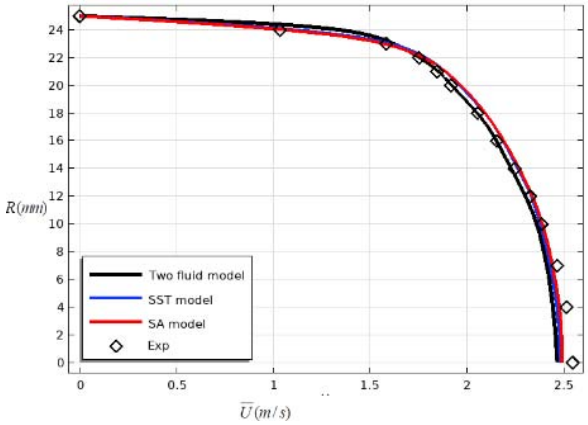

$x = 0(mm)$

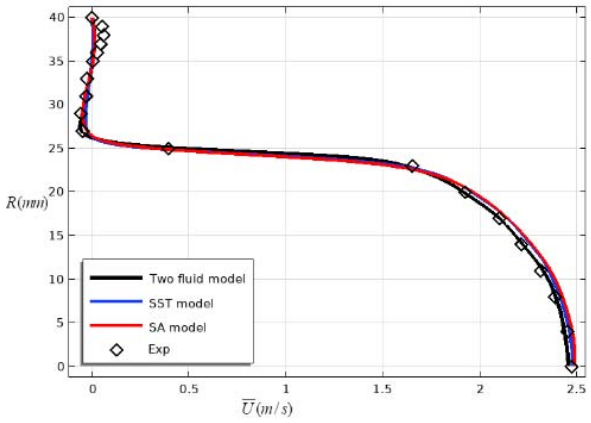

$x = 5(mm)$

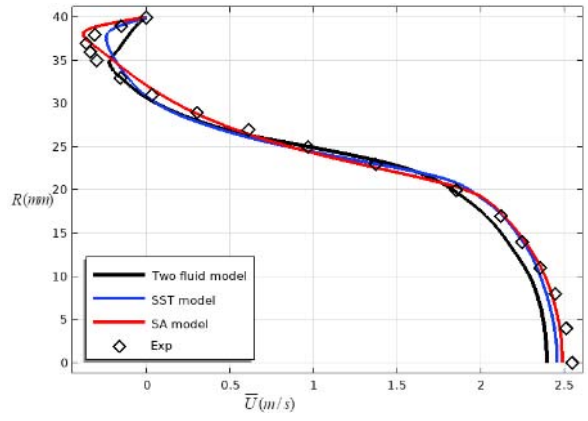

$x = 40(mm)$

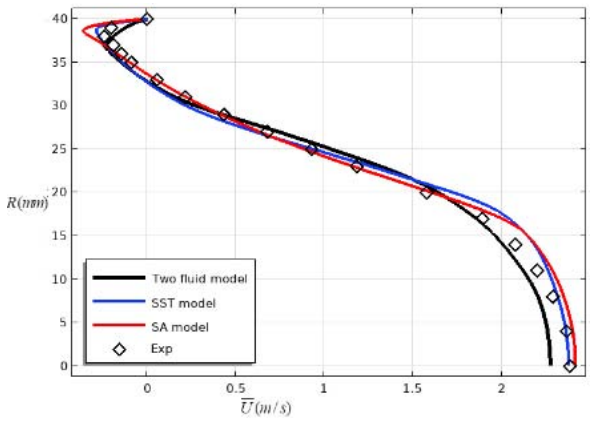

$x = 80(mm)$

Fig.10. Profiles of the axial *U*-component of flow velocity.

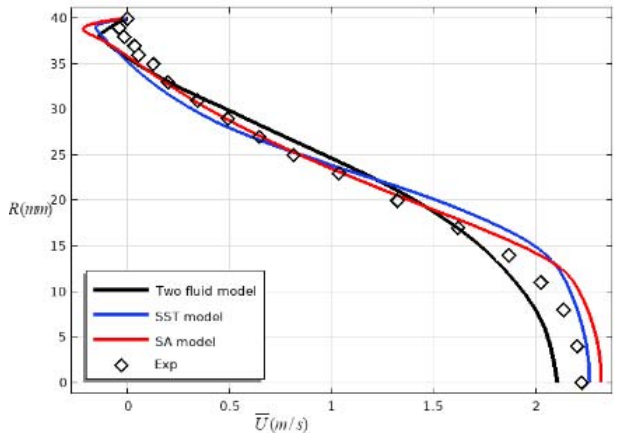

$x = 120(mm)$

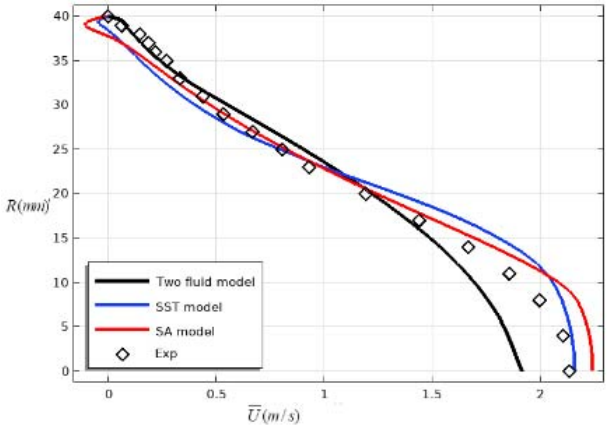

$x = 160(mm)$

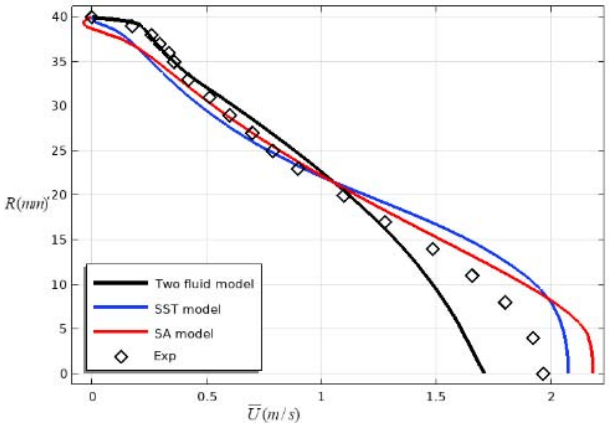

$x = 200(mm)$

Cont. Fig.10. Profiles of the axial *U*-component of flow velocity.

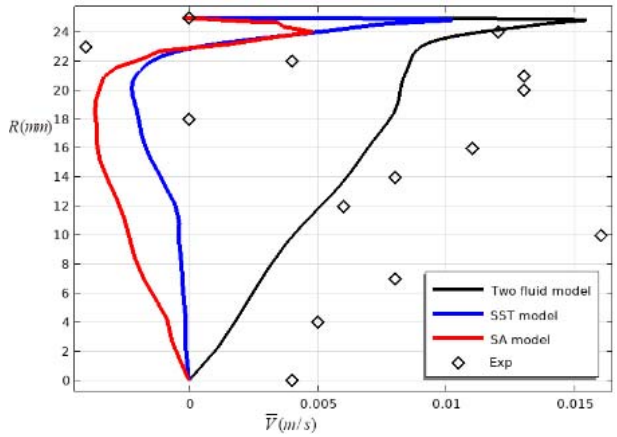

$x = 0(mm)$

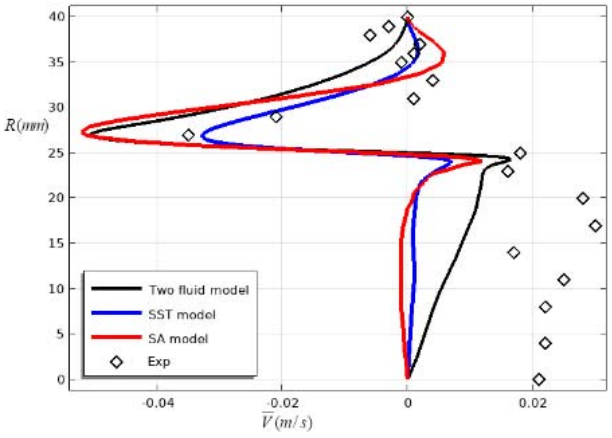

$x = 5(mm)$

Fig.11. Profiles of the radial *V*-component of the flow velocity.

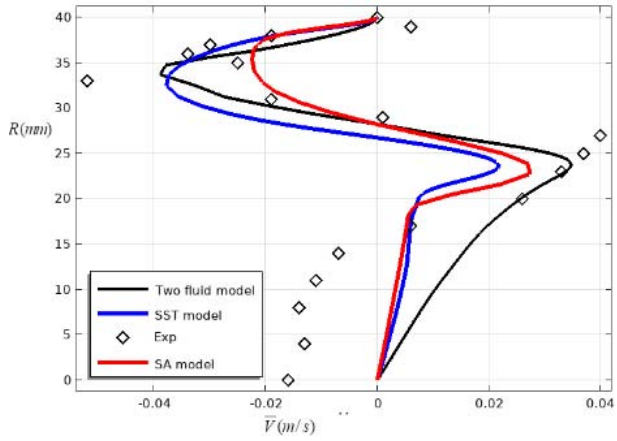

$x = 40(mm)$

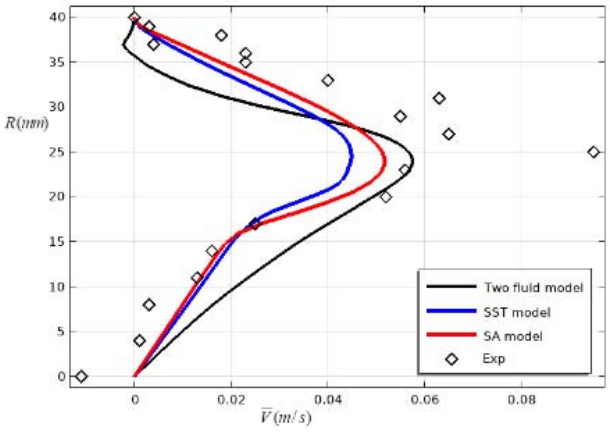

$x = 80(mm)$

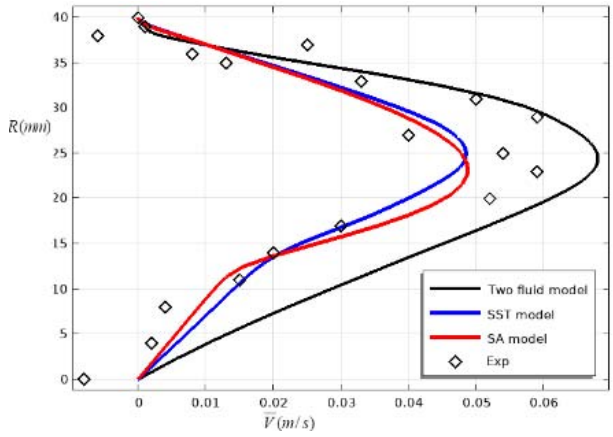

$x = 120(mm)$

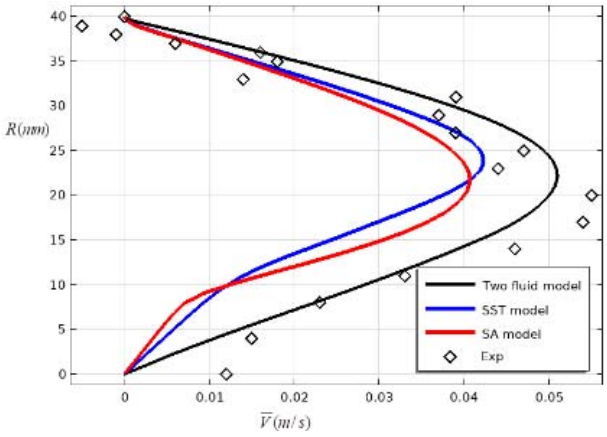

$x = 160(mm)$

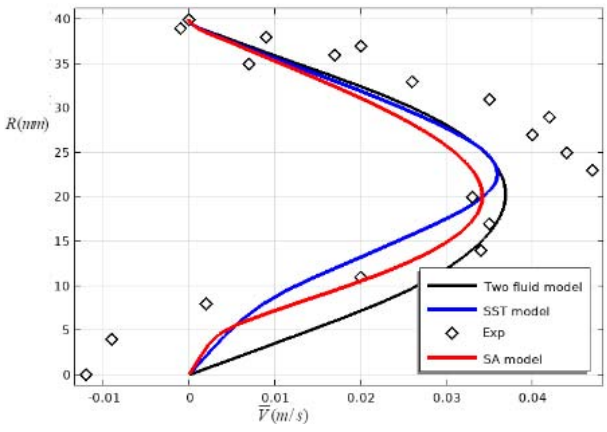

$x = 200(mm)$

Fig.11. Profiles of the radial V-component of the flow velocity.

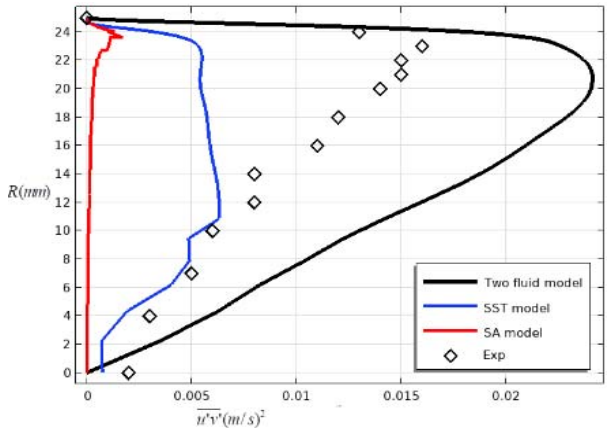

$x = 0(mm)$

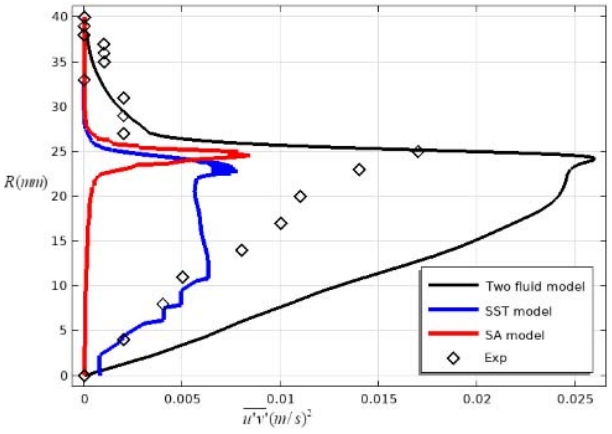

$x = 5(mm)$

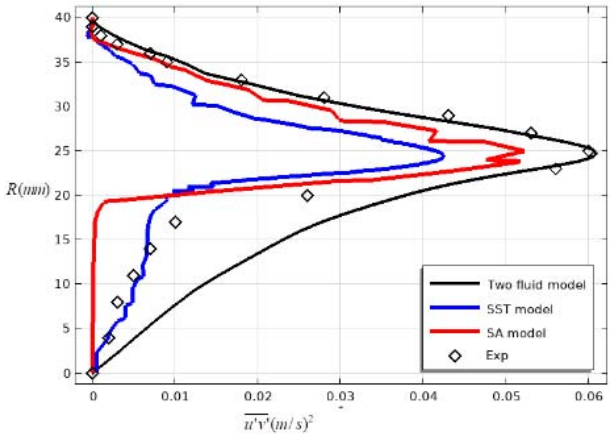

$x = 40(mm)$

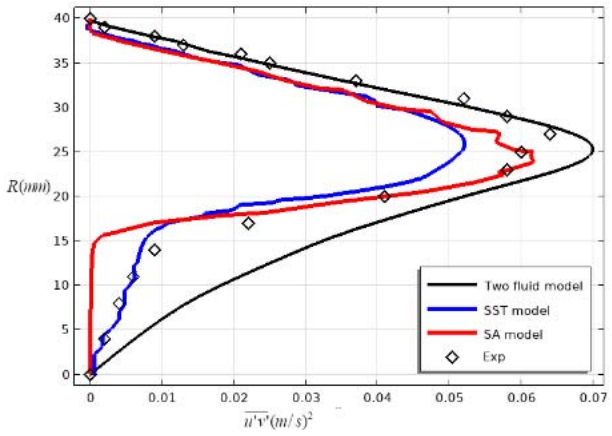

$x = 80(mm)$

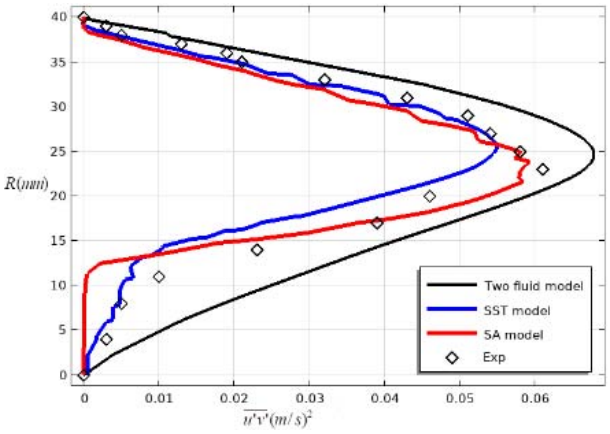

$x = 120(mm)$

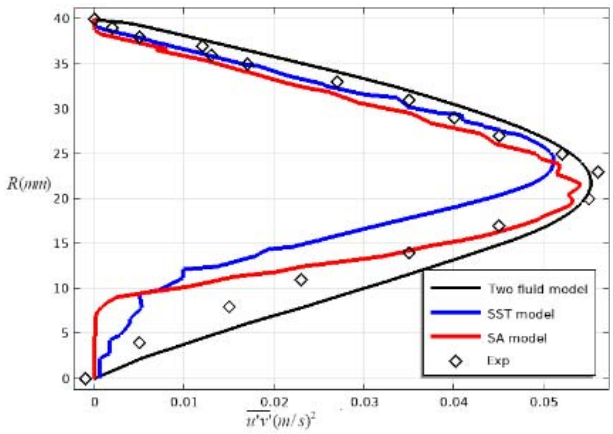

$x = 160(mm)$

Fig.12. Flow pulsation profiles *u'v'*.

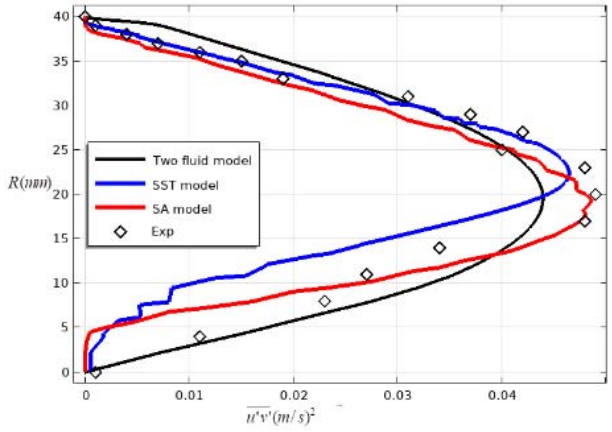

Cont. Fig.12. Flow pulsation profiles *u'v'*.

Similar results for a diffuser with an angle $\alpha = 90°$ are presented in Figs 10-12.

The flow separation and return flow zone, as well as the length of subsequent connection for all diffusers, can be more clearly represented using a plot of streamlines and velocity contours. Therefore, Fig.13 demonstrates the visualization of these processes, allowing a better understanding of the physical characteristics of the flow.

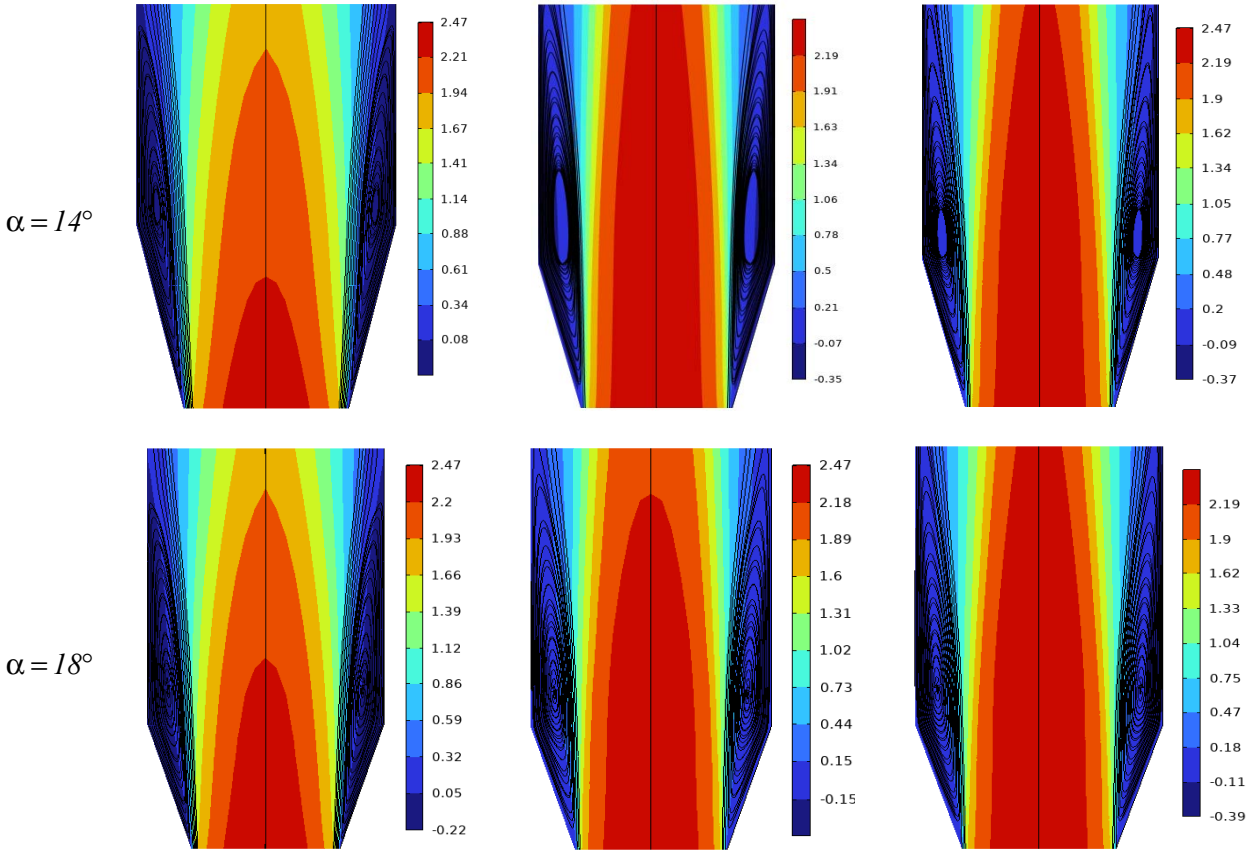

Fig.13. Isoline and flow line.

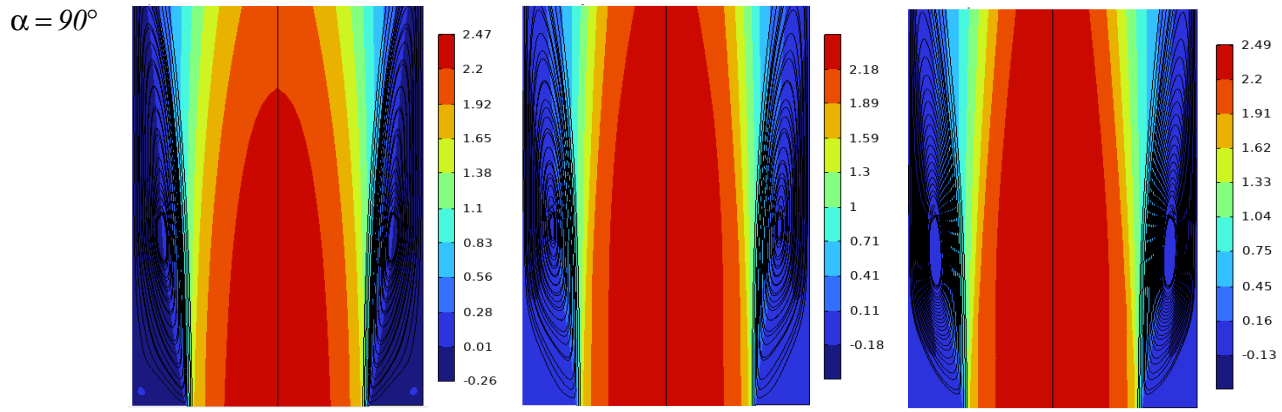

Two fluid model SST model SA model

Cont. Fig.13. Isoline and flow line.

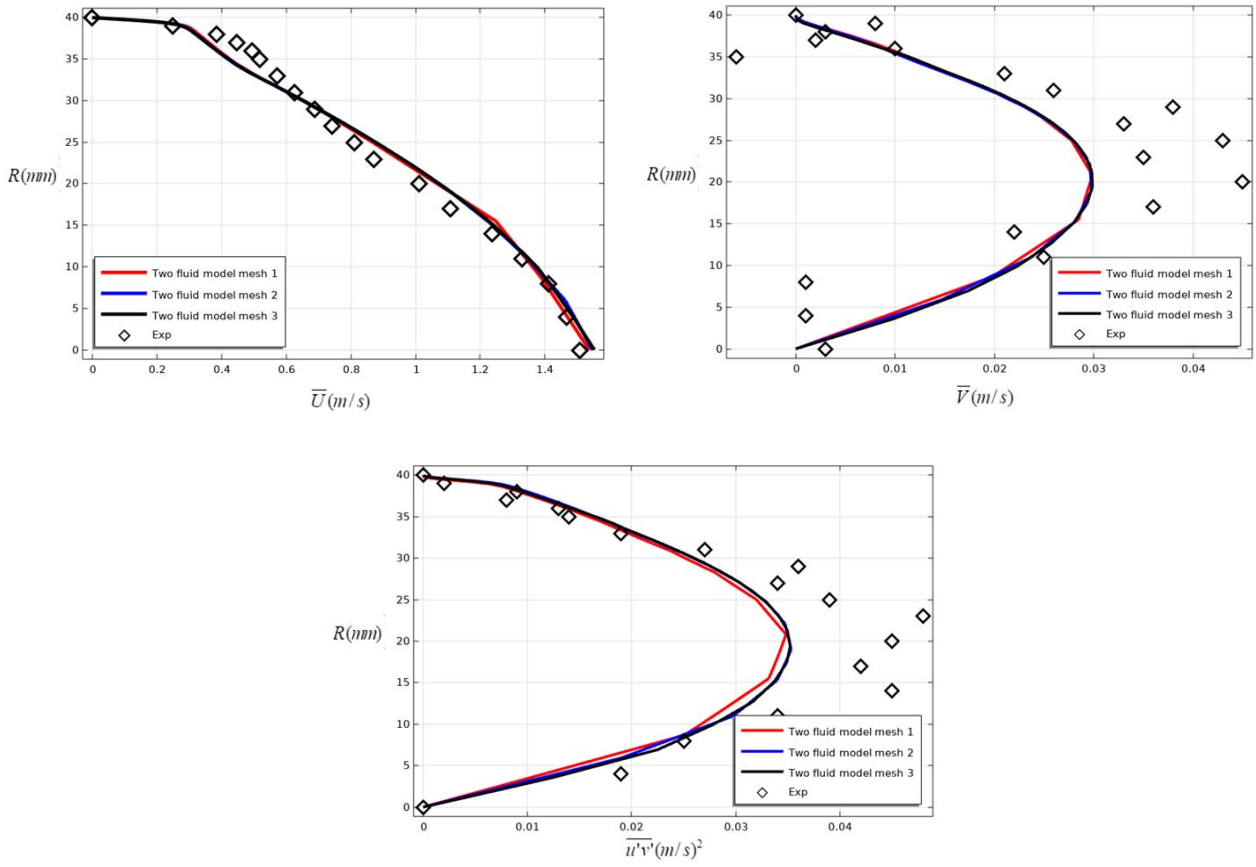

Fig.14. Influence of the mathematical model on changes in the computational mesh.

These graphs provide the ability to study and analyze flow characteristics such as separation zones and return flow zones in detail, which is extremely useful when designing or optimizing a diffuser. Visualization of changes in velocities and Reynolds voltage reveals key areas where flow separation and reflux occurs. A closer look at Fig.13 can lead to a deeper understanding of the processes occurring in a particular system. Analysis of

these graphs helps not only to identify problem areas, but also to find ways to eliminate them, which, in turn, helps to increase the efficiency and reliability of the system. This approach allows engineers and researchers to develop more optimal diffuser designs, minimizing energy loss and improving overall performance.

The influence of the mathematical model on the change in the computational mesh is an extremely important aspect. Figure 14 shows the variation of velocities and Reynolds stress at a cross section of $x = 200\ mm$ for a diffuser with an inclination angle of *14* degrees. In an axisymmetric problem, the simulation results depend on the number of nodes on the *r* axis. In this regard, three different grids were created: $1 - 300\times 20$, $2 - 300\times 30$ and $3 - 300\times 50$. The calculation of a mathematical model allows for a detailed analysis of changes in flow characteristics, such as speed and Reynolds stress, at various points of the diffuser. This is especially important for the development and optimization of engineering solutions, since the accuracy of the simulation directly affects the efficiency and reliability of the final product. Changing the number of nodes in the grid allows you to evaluate the impact of discretization on the simulation results and select the most optimal grid option for further calculations. Thus, the construction and analysis of various meshes with different numbers of nodes is an important step in the research and development of mathematical models of complex engineering systems.

5. Conclusions

As a result of the analysis of the presented data and graphs, it can be concluded that the behavior of the models differs depending on the distance from the initial section of the channel expansion. At the initial stage of expansion, all models show similar results. However, as we move away from this point, the two-fluid model turns out to be more adequate, providing more accurate agreement with experimental data. Thus, in this study, the two-fluid turbulence model is found to be an effective and accurate model for describing turbulent flow in an diverging channel. The physical significance of such analysis is that the models can more accurately predict the distribution of speeds and stresses, which are critical for the design of systems using expanding channels. For example, separation and reverse flow zones identified using a two-fluid model can be particularly important for optimizing aerodynamic performance and improving heat transfer efficiency. More accurate modeling of turbulent flows in an expanding channel allows engineers to develop designs that minimize energy loss and improve overall system performance. Additionally, the use of a two-fluid model facilitates a better understanding of the interactions between different flow components, which is important for a variety of applications including aircraft engines, piping systems and other industrial processes. This study demonstrates that the application of a two-fluid turbulent model can significantly improve the accuracy of prediction and analysis of complex flows, ultimately leading to more efficient and reliable engineering solutions.

Acknowledgements

The authors of the manuscript gratefully acknowledge the reviewers for their positive feedback and their relevant and constructive comments on our manuscript.

Nomenclature

C_1 – constant coefficient

C_2 – constant coefficient

d – closest distance to a solid wall

p – hydrostatic pressure

V_r – radial components of the averaged flow velocity vector

V_z – the axial component of the averaged flow velocity vector

λ_{max} – largest root of the characteristic equation.

ν – molar kinematic viscosity

ν' – effective molar viscosity

ρ – density

ϑ_r – radial component of fluid velocity

ϑ_z – axial component of fluid velocity

References

[1] Chang P.K.(1971): *Separation of flow*.– Elsevier, eBook ISBN: 9781483181288, p.796.

[2] John D. and Anderson J.R. (2008): *Introduction to Flight*.– McGraw-Hill, 616p.

[3] Young A.D. (1975): *Aerodynamics*.– by Clancy L.J., Pitman, pp.610, J. Fluid Mech., vol.77, No.3, pp.623-624, 1976, doi:10.1017/S0022112076212292.

[4] Cebeci T., Mosinskis G.J. and Smith A.M.O. (1972): *Calculation of separation points in incompressible turbulent flows*.– J. Aircr., vol.9, No.9, pp.618-624. https://doi.org/10.2514/3.59049

[5] Uruba V. and Knob M. (2009): *Dynamics of a boundary layer separation*.– Eng. Mech., vol.16, No.1, pp.29-38.

[6] Gustavsson J. (1998): *Experiments on turbulent flow separation*.– Masters, vol.2, p.2.

[7] Yen S.C. and Yang C.W. (2011): *Flow patterns and vortex shedding behavior behind a square cylinder*.– J. Wind Eng. Ind. Aerodyn., vol.99, No.8, pp.868-878. https://doi.org/10.1016/j.jweia.2011.06.006.

[8] Wong M.K., Sheng L.C., Azwadi C.S.N. and Hashim G.A. (2015): *Numerical study of turbulent flow in pipe with sudden expansion*.– J. Adv. Res. Fluid Mech. Therm. Sci., vol.6, No.1, pp.34-48 ISSN (online): 2289-7879.

[9] Berdanier R.A. (2011): *Turbulent flow through an asymmetric plane diffuser*.– Masters Purdue Univ. West Lafayette, Indiana, US. pp.1-35.

[10] Azad S., Riasi A., Mahmoodi Darian H. and Amiri Moghadam H. (2017): *Parametric study of a viscoelastic RANS turbulence model in the fully developed channel flow*.– Journal of Computational Applied Mechanics, vol.48, No.1, pp.65-74, DOI:10.22059/JCAMECH.2017.232031.138.

[11] Ghasemian M. and Nejat A. (2015): *Aerodynamic noise computation of the flow field around NACA 0012 airfoil using large eddy simulation and acoustic analogy*.– Journal of Computational Applied Mechanics, vol.46, No.1, pp.41-50, DOI:10.22059/JCAMECH.2015.53392.

[12] Javanbakht A. and Ahmadi Danesh Ashtian H. (2018): *Impeller and volute design and optimization of the centrifugal pump with low specific speed in order to extract performance curves*.– Journal of Computational Applied Mechanics, vol.49, No.2, pp.359-366, DOI: 10.22059/JCAMECH.2018.246099.211

[13] Chandavari V. and Palekar S. (2014): *Diffuser angle control to avoid flow separation*.– Int. J. Tech. Res. Appl., vol.2, No.5, pp.16-21.

[14] Fakhar M.H., Fakhar A., Tabatabaei H. and Nouri-Bidgoli H. (2020): *Investigation of instable fluid velocity in pipes with internal nanofluid flow based on Navier-Stokes equations*.– Journal of Computational Applied Mechanics, vol.51, No.1, pp.122-128, DOI:10.22059/JCAMECH.2020.300244.496.

[15] Noghrehabadi A., Daneh Dezfuli A. and Alipour F. (2019): *Solving single phase fluid flow instability equations using Chebyshev Tau-QZ polynomial*.– Journal of Computational Applied Mechanics, vol.50, No.1, pp.135-139, DOI:10.22059/JCAMECH.2018.250600.235.

[16] Abdelkarim B. and Djedid T. (2019): *Numerical investigation of natural convection phenomena in uniformly heated trapezoidal cylinder inside an elliptical enclosure*.– Journal of Computational Applied Mechanics, vol.50, No.2, pp.315-323, DOI: 10.22059/JCAMECH.2019.291495.442.

[17] Le H., Moin P. and Kim J. (1997): *Direct numerical simulation of turbulent flow over a backward-facing step*.– J. Fluid Mech., vol.330, pp.349-374, DOI: https://doi.org/10.1017/S0022112096003941.

[18] Durst F., Melling A. and Whitelaw J.H. (1974): *Low Reynolds number flow over a plane symmetric sudden expansion*.– J. Fluid Mech., vol.64, No.1, pp.111-128, DOI: https://doi.org/10.1017/S0022112074002035.

[19] Cherdron W., Durst F. and Whitelaw J.H. (1978): *Asymmetric flows and instabilities in symmetric ducts with sudden expansions*.– J. Fluid Mech., vol.84, No.1, pp.13-31, DOI: https://doi.org/10.1017/S0022112078000026.

[20] Törnblom O., Herbst A. and Johansson A.V (2004): *Separation control in a plane asymmetric diffuser by means of streamwise vortices experiment, modelling and simulation*.– in The 5th Symposium on Smart Control of Turbulence, pp.1-21.

[21] Stieglmeier M., Tropea C., Weiser N. and Nitsche W. (1989): *Experimental investigation of the flow through axisymmetric expansions*.– J. Fluids Eng. Trans. ASME, vol.111, No.4, pp.464-471, doi: 10.1115/1.3243669.

[22] Sagar D., Paul A.R. and Jain A. (2011): *Computational fluid dynamics investigation of turbulent separated flows in axisymmetric diffusers*.– Int. J. Eng. Sci. Technol., vol.3, No.2, DOI:10.4314/ijest.v3i2.68138, pp.104-109.

[23] Malikov Z. (2020): *Mathematical model of turbulence based on the dynamics of two fluids*.– Appl. Math. Model., vol.82, pp.409-436, https://doi.org/10.1016/j.apm.2020.01.047.

[24] Malikov Z.M. and Madaliev M.E. (2021): *New two-fluid turbulence model based numerical simulation of flow in a flat suddenly expanding channel*.– Her. Bauman Moscow State Tech. Univ. Ser. Nat. Sci., No.4, doi: 10.18698/1812-3368-2021-4-24-39.

[25] Madaliev M.E. (2023): *Numerical simulation of turbulent flows on the basis of a two-fluid model of turbulence*.– Vestn. Tomsk. Gos. Univ. Mat. i Mekhanika, No.82, doi: 10.17223/19988621/82/10.

[26] Malikov Z.M. and Madaliev M.E. (2021): *Numerical simulation of flow in a two-dimensional flat diffuser based on two fluid turbulence models*.– Comput. Res. Model., vol.13, No.6, doi: 10.20537/2076-7633-2021-13-6-1149-1160. DOI: 10.20537/2076-7633-2021-13-6-1149-1160.

[27] Menter F. (1993): *Zonal two equation kw turbulence models for aerodynamic flows*.– in 23rd Fluid Dynamics, Plasmadynamics, and Lasers Conference, p.2906. https://doi.org/10.2514/6.1993-2906.

[28] Spalart P. and Allmaras S. (1992): *A one-equation turbulence model for aerodynamic flows*.– in 30th Aerospace Sciences Meeting and Exhibit, p.439, https://doi.org/10.2514/6.1992-439.

[29] Spalart P.R. (1997): *Comments on the feasibility of LES for wings and on the hybrid RANS/LES approach*.– in Proceedings of the First AFOSR International Conference on DNS/LES, pp.137-147, CRID 1571698601146488576.

[30] Patankar S. (2018): *Numerical Heat Transfer and Fluid Flow*.– Taylor & Francis, https://doi.org/10.1201/9781482234213.

[31] Menter F.R. (2002): *Methoden, Moeglichkeiten und Grenzen numerischer Stroemungsberechnungen*.– Numet. Erlangen, pp.1-15.

[32] Kholboev B.M., Navruzov D.P., Asrakulova D.S., Engalicheva N.R. and Turemuratova A.A. (2022): *Comparison of the results for calculation of vortex currents after sudden expansion of the pipe with different diameters*.– International Journal of Applied Mechanics and Engineering, vol.27, No.2, pp.115-123, https://doi.org/10.2478/ijame-2022-0023.

Received: May 8, 2024
Revised: July 25, 2024